Simulation of the primary breakup of non-Newtonian liquids at a high-speed rotary bell atomizer for spray painting processes using a VOF-Lagrangian hybrid model

B. Shen*[1], Q. Ye[2], O. Tiedje[2], J. Domnick[1]
[1]University of Applied Sciences Esslingen, Esslingen, Germany
[2]Fraunhofer Institute for Manufacturing Engineering and Automation, Stuttgart, Germany
*Corresponding author: bo.shen@hs-esslingen.de

Abstract
The present contribution deals with numerical and experimental studies of the primary liquid breakup process using a high-speed rotary bell atomizer. The investigation focuses on the disintegration process of the paint liquid in the near-bell region. A hybrid multiphase model that links the Volume of Fluid (VOF) model and the Discrete Phase Model (DPM) is implemented in the CFD software ANSYS Fluent. In the simulation, the VOF model tracks the liquid-gas interface to describe the flow of the liquid film on the bell and the liquid disintegration at the bell edge. Under the given conditions, the developed hybrid model converts the liquid lumps resulting from the VOF-solver into point masses that can be further tracked using the DPM model. Moreover, droplet properties such as volume, equivalent diameter, velocity and position can be determined with the DPM statistics. The resulting quantitative simulation data, i.e. drop velocities and droplet size distributions, are compared with the experimental results applying Laser Doppler Anemometry (LDA) and laser diffraction instruments.

Keywords
Primary breakup, numerical simulation, rotary bell atomizer, liquid disintegration, VOF-Lagrangian hybrid model

Introduction

High-speed rotary bell atomizers are widely used in automated painting processes. Compared to rotary atomizers used in other applications, e.g., spray drying or powder production, rotary atomizers for painting are characterized by small bell diameters varying between 20 and 70 mm and very high rotary speeds of the bell of up to 70,000 min^{-1}. They provide excellent paint film quality as well as high transfer efficiencies due to electrostatic support and the possibility to control droplet size and droplet transport separately. However, the influence of complex material properties on atomization is still an open research topic.

In general, some research work has already been done to investigate the atomization with rotary atomizers (e.g. [1-3]). There are also a few publications presenting results from experimental work [4] dealing with high-speed rotary bells used in painting processes. Domnick et al. [5] presented numerical investigations aiming to calculate the two-phase flow field inside the paint supply system of a rotary bell atomizer and the formation of the free film on the bell surface. However, the cell resolution of the computational domain was quite limited due to the previously available low computational capacity. The viscosity of the paint used in their investigation was chosen to be constant, i.e., the non-Newtonian behavior which most of real paint materials exhibit was not taken into consideration. In our previous work [6], a significantly finer mesh was used in the numerical investigations, and the shear-thinning behavior of the paint material was also considered. The process of the paint propagating from the disk to the bell could be observed. The blocking effect of the bolts, by which distributor disk and bell are assembled together, plays an important role in this process. The paint leaves the distributor disk in form of drops or ligaments, reaches the inner surface of the bell and builds a film on it. The paint flows further along the inner surface towards the bottom edge of the bell. After a certain time, the inner surface of the bell is completely wetted by the paint. However, the distribution of the film thickness is not homogeneous. Subsequently, our recent work [7] focused more on the region near the bell edge, where liquid atomization occurs. Numerical simulations were carried out using an even finer mesh around the bell edge. The computational domain was limited to the close vicinity of the bell edge in order to save computational consumption. Depending on the paint flow rate and rotary speed of the bell, regimes of droplet and ligament formation during the liquid disintegration process could be found in the simulations. User defined functions (UDFs) were developed and compiled in ANSYS Fluent to determine the sizes, positions and velocities of drops, so that drop size distributions in the whole computational domain could be plotted. However, it is very challenge to sample VOF drops at given cross sections as that is usually done in experiments... Hence, in this respect the simulation results could not be used for comparison with the experimental data.

In the present contribution, the VOF-DPM hybrid model in the commercial CFD code ANSYS Fluent is used to investigate and analyze the liquid breakup. Due to the VOF-DPM model transition mechanism, sampling particles at any given cross section is also possible in the simulation. However, to sensibly apply this hybrid model in the present investigations, appropriate values for the various criteria in the model had to be determined. The mesh sensibility of the hybrid model is also analyzed. The resulting simulation results can be compared with experimental data.

Characteristics of the atomizer

The investigations presented in this paper were carried out with a high-speed rotary bell atomizer by EISENMANN LacTec GmbH which is used in automated paint applications. Figure 1 shows the CAD model of the atomizer and a cross section of the bell. Paint liquid is injected through an orifice which has a narrow diameter of 1.6 mm. This paint supply nozzle is surrounded by an annular gap with a width of 0.5 mm, through which ambient air is sucked down. This gas flow helps to form an initial stable fluid film on the bell and to prevent the formation of ligaments on the bell surface, so that the atomization quality could be improved [8]. Downstream the paint supply nozzle, there is an inner distributor disk with a diameter of 20 mm. The distributor disk and the bell are assembled together using three bolts. During application they both rotate at high speed, while the paint supply nozzle remains static. The paint is injected onto the distributor disk and builds a paint film on it. The paint film is further radially accelerated by centrifugal forces and eventually becomes unstable at a certain distance from the rotating axis. Finally, the paint becomes distributed on the distributor disk surface as well as the inner surface of the bell. Airflows coaxial with the bell emerging from two rings of air nozzles behind the bell, referred to as inner and outer shaping air flows, are involved to shape the paint spray and to transport the droplets toward the substrate to be coated. Each of their flow rates can individually be adjusted.

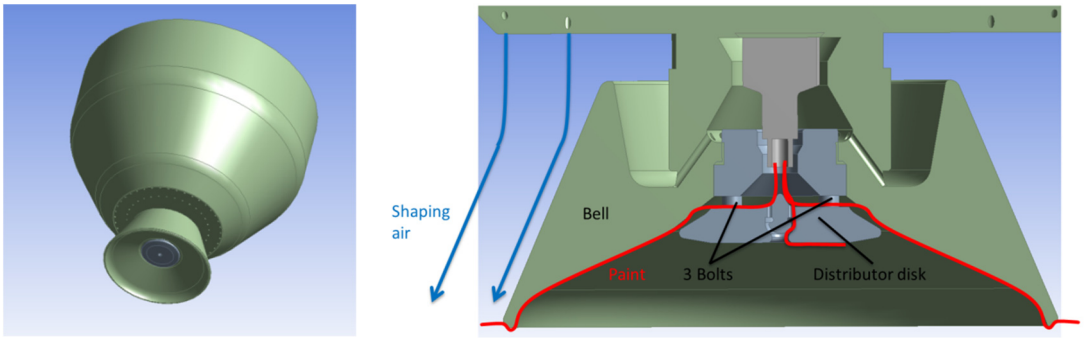

Figure 1. CAD model of the rotary bell atomizer (left) and cross section of the bell (right)

Rheological properties of the paint

For the investigations shown here, a real paint used in automated painting processes was chosen whose viscosity, experimentally measured by rotational and capillary viscometers, is plotted as a function of the shear rate in Figure 2. The paint shows shear-thinning behavior, i.e., the viscosity decreases with increasing shear rate. This kind of non-Newtonian behavior was also applied in the simulations. The correlation between viscosity and shear rate is described by using a power law model, in this case the Cross model [9], which is also plotted in Figure 2.

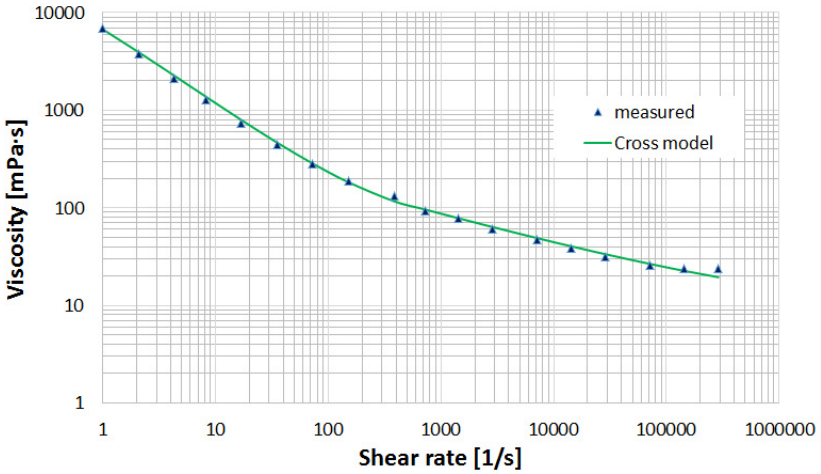

Figure 2. Correlation between viscosity and shear rate of the paint used in the investigations

Numerical methods

The computational domain used in the present investigation is shown in Figure 3. Here, only 1/64 of the bell area was used. A small section of the inner bell surface was retained. Through the normal section at a distance of 1 mm from the bell bottom, the paint material flows into the computational domain in form of a liquid film. The wall boundary of the bell is extended around the fillet on the outer bell surface. The domain is enlarged laterally by 4 mm to the fillet and downwards by 2 mm. The upper surface of the computational domain was defined as a shaping air inlet to consider the effect of the shaping air on the disintegration process.

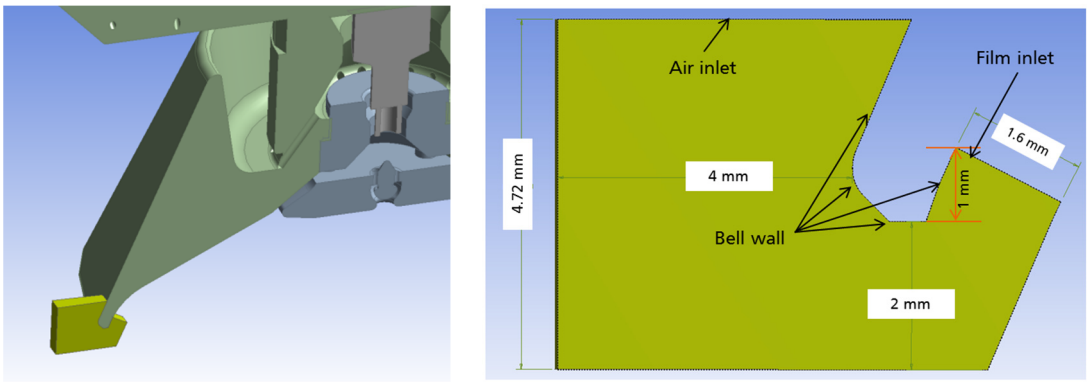

Figure 3. Computational domain

A cross-section of the meshed computational domain is shown in Figure 4. The whole computational domain could be built using structured grids. On Figure 4 (left) it is shown that the domain was sliced into three parts with different refinement of the mesh. The region (1) near the bottom edge of the bell, where the primary breakup occurs, was meshed with a grid size of 10×10×10 µm. Prism layers were created both on the inner and outer surface of the bell. The height of the first prism layer close to the bell is 5 µm, which provides the necessary resolution for the calculation of the film thickness on the bell. The growth rate of the prism layers was chosen as 1.2. Under shaping air conditions, no liquid, neither in form of a film nor in form of droplets, can enter into the region (3) above the fillet on the outer bell surface. Hence, a VOF calculation was not carried out in this region and a courser grid size of 30×40×40 µm could be used to save computational consumption. In the remaining domain (2), a medium grid of 10×20×20 µm was generated. The overall mesh cell count was about 17 million. This mesh is further called the basic mesh. The region (1) was partially refined to gain a refined mesh for examining the mesh sensitivity of the VOF-DPM hybrid model. The refined region has a grid size of 5x5x5 µm. The liquid disintegration and the conversion from VOF liquid to DPM particles will mostly occur in this region. The total of cell elements in the refined mesh amounts to approx. 30 million.

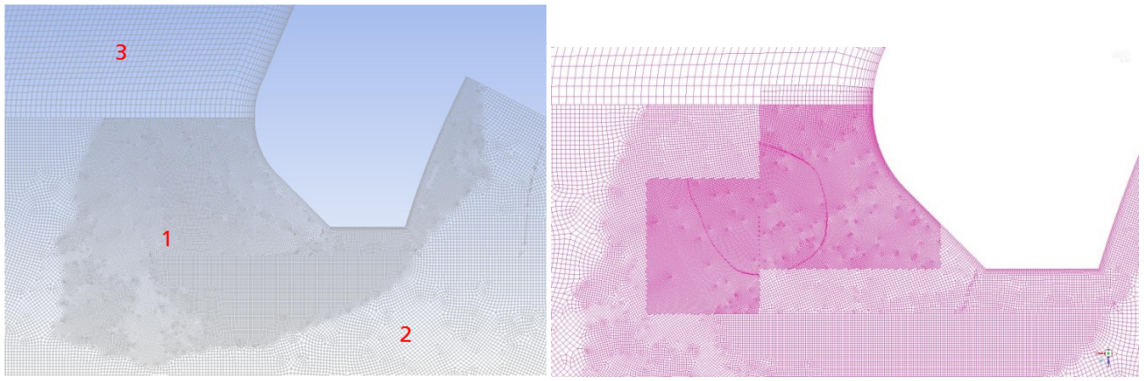

Figure 4. Computational mesh, left: basic mesh and right: refined mesh

The numerical simulations were carried out using the commercial CFD code ANSYS Fluent based on the finite-volume approach. The code provides a model transition mechanism to combine the Volume of Fluid (VOF) model and the Discrete Phase Model (DPM). In the simulation, the VOF model tracks the liquid-gas interface to describe the flow of the liquid film on the bell and the liquid disintegration at the bell edge. The hybrid model finds liquid lumps that are detached from the liquid film. Under the given conditions, such as lump size and asphericity, the liquid lumps are removed from the VOF-solver and converted to point masses in the Lagrangian formulation that can be further tracked using the DPM model. For time-dependent VOF calculations, variable time stepping was used in order to automatically change the time step when an interface is moving through dense cells or when the interface velocity is high. The time step was varied in a range between 0.1 and 1 µs based on the preconfigured maximum global Courant number of 2, which ensures the computational stability of the numerical simulations.

Boundary conditions

As mentioned above, the wetting process on the bell was not calculated in the present investigations. Instead, the properties of the paint film in the normal section of the inner bell surface were given as input parameters. Thickness and flow velocities of the paint film could be obtained in the wetting simulations that were carried out in our previous work [6]. For instance, in the case of a paint flow rate of 250 ml/min and a bell rotary speed of 55,000 min^{-1}, 16.1 µm for the thickness of the paint film at the inlet and 1.58 m/s for the mean velocity of the film were used as appropriate values.

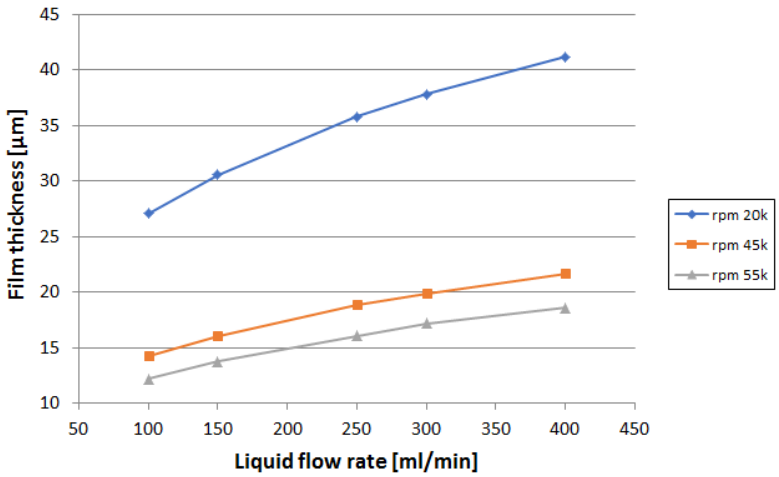

Figure 5. Correlation between film thickness and liquid flow rate taken from previous work [6]

Criteria of the hybrid model

Asphericity is a shape based criterion used by the VOF-to-DPM model to identify lumps which can be converted from the resolved liquid using the VOF model to particles tracked with the DPM model. Asphericity indicates the deviation from the shape of a perfect sphere. Therefore, the value of asphericity is zero for perfect spheres. Asphericity values of lumps are detemined in two ways, namely calculated from normalized radius standard deviation and average radius-surface orthogonality. In the first way, the standard deviation of the distance between the boundary facet center and the lump center of gravity is computed and then normalized by the average radius. To yield the other asphericity quantity, the vector from the lump center of gravity to the center of

the lump boundary facet is computed and then used in a dot product with the facet unit normal. In the simulation, it is allowed to specify the maximum asphericity value for both calculation methods. Only lumps for which the asphericity value is below the specified maximum can be elected for conversion from the VOF liquid to DPM particles.

The simulation results for three cases with different specified maximum asphericity are shown in Figure 6. A paint flow rate of 250 ml/min and a rotary speed of 55,000 min^{-1} are thereby used. For the case shown in Figure 6a, the maximum asphericity is 0.5, 0.25 for Figure 6b and 0.1 for Figure 6c. The VOF liquid is indicated in magenta and the DPM particles are shown in a color selected from blue to red depending on their sizes.

At the high asphericity upper limit, the majority of VOF liquid can be converted to DPM particles directly at the bell edge, and no more VOF lumps indicated in magenta can be observed downstream. In contrast, only VOF liquid can be found directly at the bell edge in the simulation with the low asphericity upper limit, and the conversion from the VOF liquid to DPM particles occurs later. VOF liquid can also be seen downstream in the computational domain und even on the bottom border. At the asphericity upper limit of 0.1, only approximately 80% of the injected mass is converted to DPM particles, while more than 95% of the injected mass can be tracked in the form of DPM particles for the maximum asphericity of 0.5.

Significantly different spray angles can be observed in the simulations. In the case with the maximum asphericity of 0.5, the particle conversion occurs directly at the bell edge. The initial velocities of the DPM particles are very high and approximately equal to the tangential velocity of the rotary bell. However, the axial component of the initial particle velocities is about equal to zero. When liquid particles are converted from irregularly shaped VOF lumps to spherical DPM particles, the drag force caused by the shaping air on them will be underestimated in the DPM tracking process. Therefore, almost all particles fly approximately horizontally in the left direction and leave the computational domain through the left border. With decreasing upper limit of asphericity, liquid particles are tracked longer with the VOF solver und the shaping air has more effect on them. More particles can be dragged down and fly through the bottom border of the computational domain. However, the majority of particles leave the domain through the left border until the maximum asphericity is specified to 0.1. Under the same conditions, the paint spray was recorded by means of a high-speed camera and shown in Figure 6d. Although the boundary line of the spray cannot be clearly determined due to the blurring of the image caused by the high velocities of particles, a significant angle between it and the horizontal line can observed. Only a few particles fly horizontally towards the left side. Thus, the maximum asphericity of 0.1 appears to be an appropriate value for the present investigation.

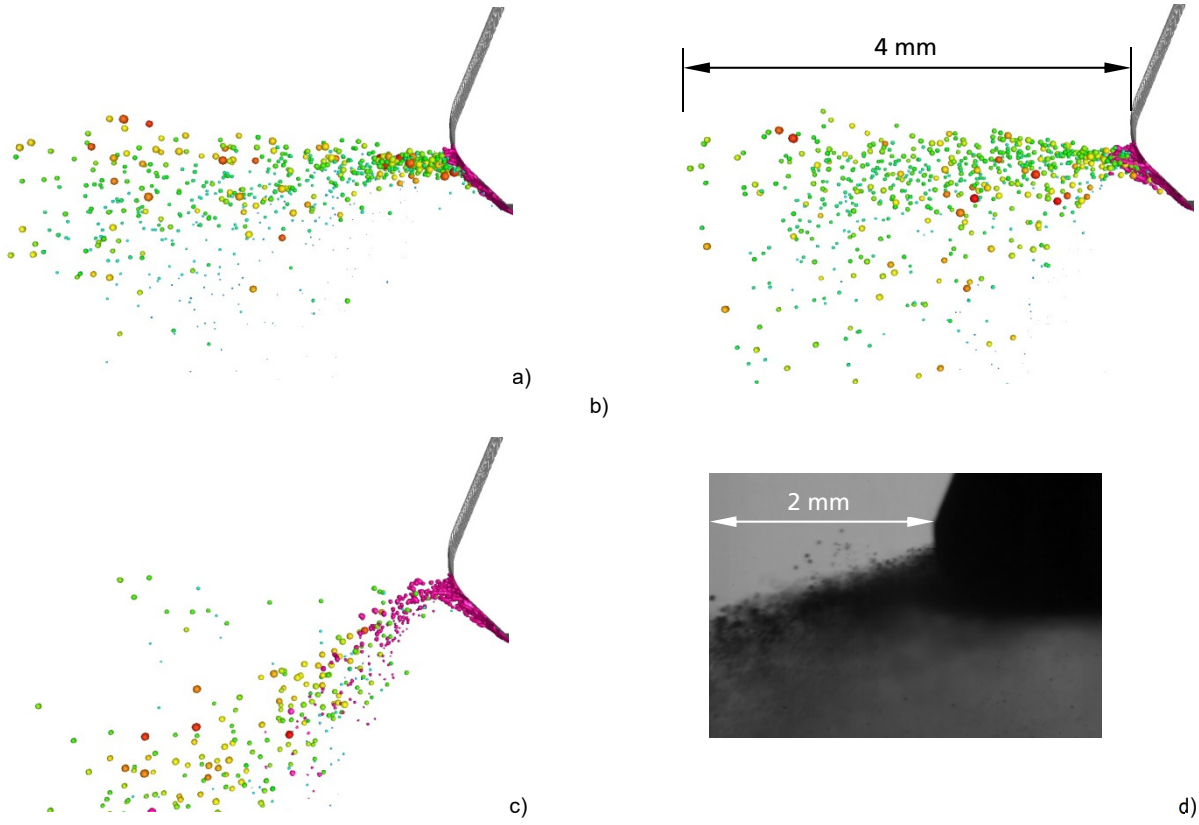

Figure 6. Simulation results under different upper limits of asphericity a) 0.5; b) 0.25; c) 0.1 and d) visualization using a high-speed camera

Particle distributions

Under the determined upper limit of asphericity of 0.1, the disintegration process of the paint liquid was calculated with both the basic and refined mesh. After the spray has completely developed, the simulations were further carried out for a longer time to sample all particles that fly through the given cross sections, e.g., z = 2 mm downstream from the bottom edge of the bell. Figure 7 shows the probability density functions of both mass distribution and number distribution in the particle diameter space at z = 2 mm, using the basic and refined mesh, respectively. In both simulations, quasi-normal mass distributions can be obtained. However, by refining the mesh the distributions are significantly shifted to the left (smaller droplets). The maximum simulated particle sizes are 49 µm for the basic mesh and 39 µm for the refined mesh. For the refined mesh particles in the range of 10 to 30 µm provide the majority of the mass. For the simulation with the basic mesh particles from 25 to 45 µm are dominant. A certain number of very small particles, namely smaller than 2 µm, can be observed in the simulations. Clearly, additional investigations are necessary to clarify if these small particles are simply the result of numerical diffusion. Fortunately, they can be mainly ignored in the coating process as their contribution to the resulting film thickness on the substrate is negligible due to the low mass fraction.

The Sauter mean diameter (SMD) is determined to be 29.5 µm for the basic mesh and 17.6 µm for the refined mesh. Unfortunately, sensible particle size measurements in the considered dense regions of the spray, e. g., using laser diffraction instruments, could not be performed successfully with the necessary spatial resolution. Also, it should be noted that phase-Doppler anemometry, which could provide appropriate data, cannot be applied due to optical inhomogeneities of many real paints. So far, comparisons are only possible with size measurements further downstream at larger distances from the bell. At z = 25 mm from the plane of the bell edge the measured SMD is 11.0 µm, at z = 50 mm it is 8.6 µm. The experimental SMDs are smaller than the SMDs from the simulations, and decrease with increasing distance from the bell. Considering the obtained evolution of the SMD as a function of the distance, the primary particle distribution provided by the simulation with the refined mesh seems to be reasonable.

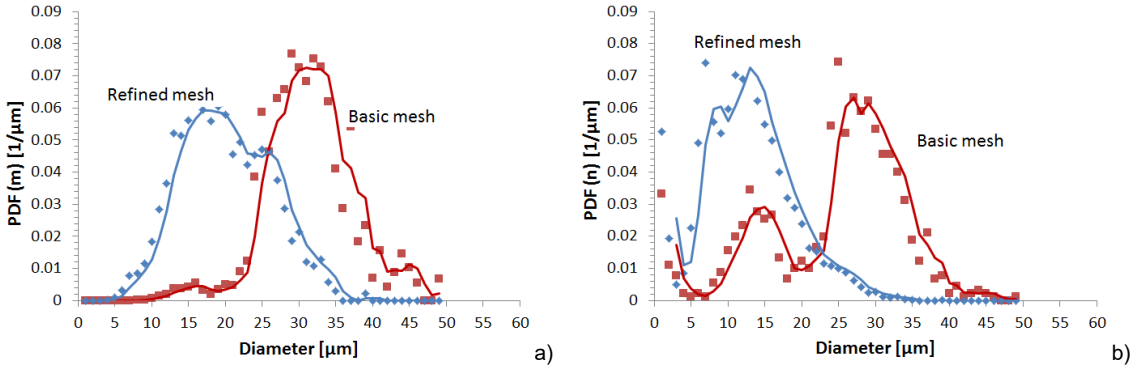

Figure 7. Probability density function of a) mass distribution and b) number distribution in the particle diameter space

Particle velocities

The correlation between particle sizes and velocities, namely velocity magnitude and three components of velocity, can also be obtained from the simulations. Based on the sampling data from the simulation with the refined mesh, the results are plotted in Figure 8. In general, the velocities of the particles increase with increasing particle size. With respect to the individual velocity components, the correlation is rather weak for the axial velocity but much more distinct for the radial and the tangential components. In the case of the radial component, the velocities between smallest and largest droplets differ by more than a factor of 2.

Furthermore, the velocities of particles that are located at the same position in the cross section z = 2 mm were averaged independently of particle size. In Figure 9, the resulting evolution of the particle velocity along the x coordinate is compared with experimental data measured by means of Laser Doppler Anemometry (LDA). Due to remaining uncertainties in the positioning of the measuring planes, the numerical results are compared with experimental data from z = 1 mm and z = 2 mm.

For the axial velocities, a very good agreement between the simulation result and the LDA data can be obtained. The axial velocity component of the particles very close to the bell edge is low but increases significantly with increasing distance from bell edge. At a distance of 3 mm, the axial velocity of the particles rises to the maximum value of approx. 35 m/s and decreases afterwards along the x coordinate. The radial velocities increase along the x coordinate both in the simulations as well as in the experiments up until a distance of 5 mm from the bell edge. However, up to a distance of 2 mm the radial velocity in the simulations is smaller than the LDA data. The radial

velocity rises more quickly in the simulations and subsequently lies between the experimental values obtained at z = 2 mm and z = 1 mm. For the tangential velocities, a significant difference between the simulation results and the LDA data at z = 2 mm can be observed. The values resulting in the simulations are similar to the LDA values at z = 1 mm, but they cannot represent the evolution of the tangential velocities observed in the experiment.

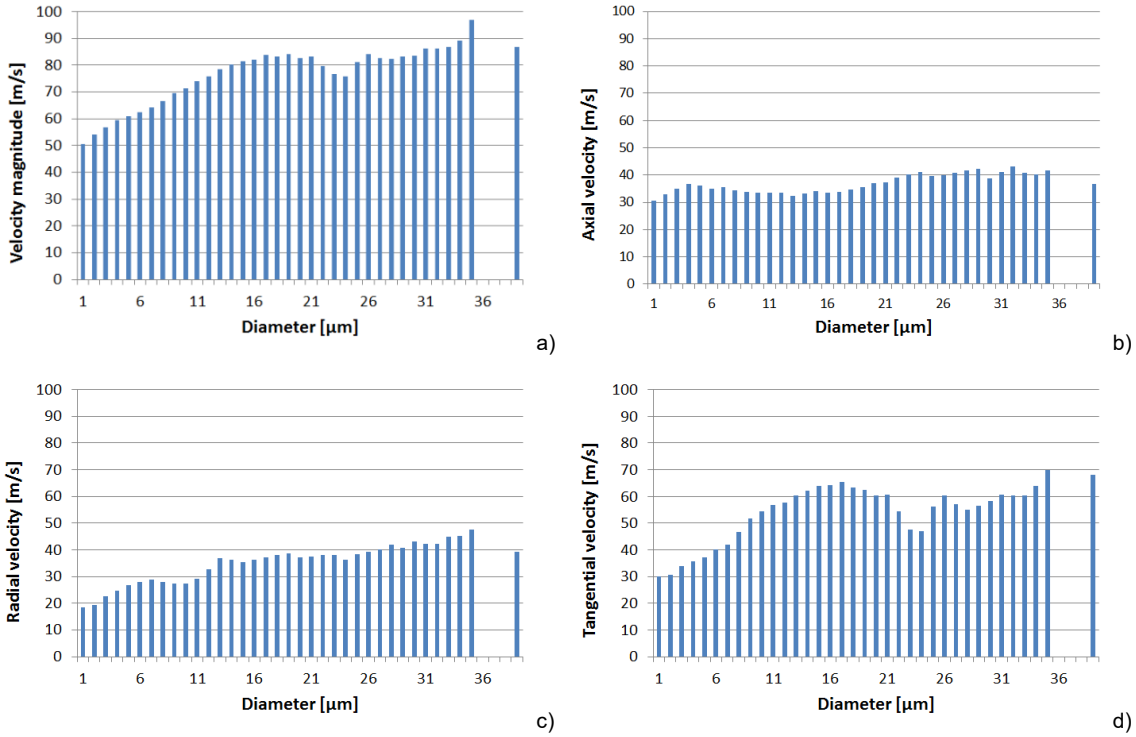

Figure 8. Correlation between particle sizes and velocities

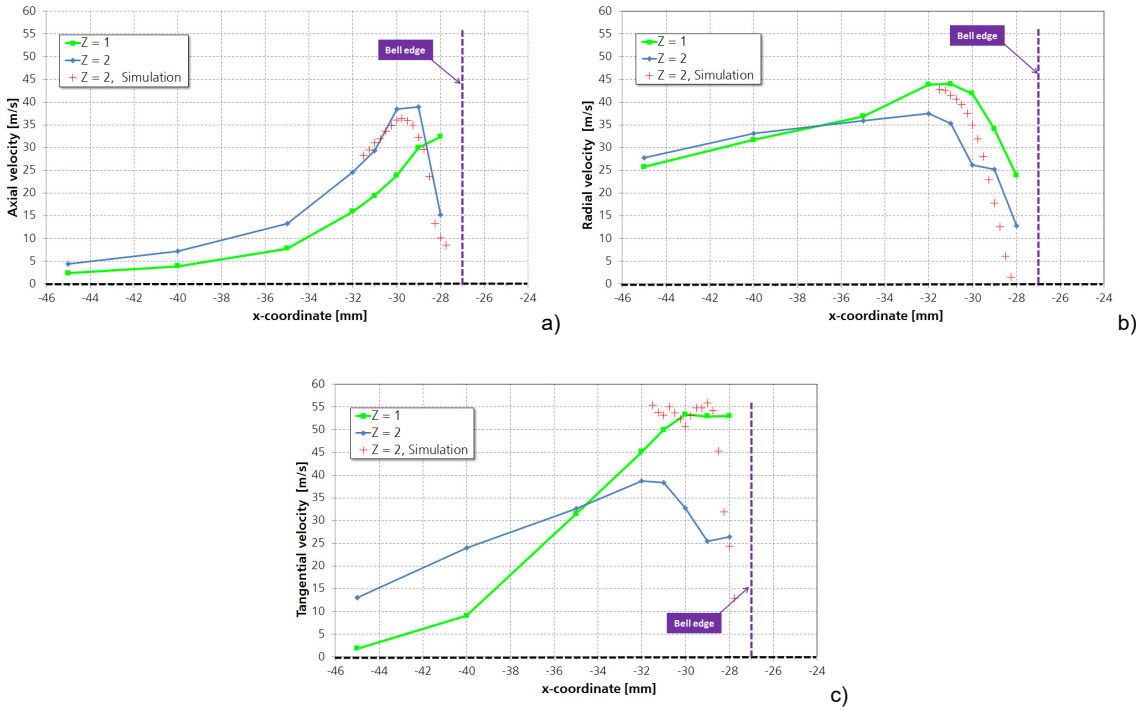

Figure 9. Comparison of particle velocities with experimental data

Conclusions

As presented in this paper, numerical simulations based on the VOF-DPM hybrid model were carried out to study the paint disintegration near the rotary bell. The results of previous wetting simulations were used as input conditions. A reasonable value for the shape-based criterion, namely the upper limit of asphericity, of the hybrid model was found in the present investigations. The mesh sensitivity of the hybrid model was also analyzed. It is concluded that the refined mesh can provide a more realistic primary particle distribution. Based on the sampling data from the simulations, positive correlations between particle sizes and velocities can be determined. Furthermore, particle velocities from the simulations can be compared with the experimental data measured using Laser Doppler Anemometry (LDA).

In future studies we will extend the bottom boundary of the computational domain to a value of 25 mm downstream the bottom edge of the bell. Clearly, in this situation it will be necessary to include a realistic model for the secondary breakup process in the simulations. Hopefully, it will be possible to improve the quality of the comparison between simulated and experimentally obtained size distributions and mean droplet diameters by applying a reasonably good model for secondary droplet breakup.

Acknowledgements

The present investigations were supported by the Arbeitsgemeinschaft industrieller Forschungsvereinigungen (AIF). The work has also been supported by the High-Performance Computing Center (HLRS) of the University of Stuttgart (German federal project: PbusRobe). We thank our colleagues from the Fraunhofer Institute for Manufacturing Engineering and Automation in Stuttgart who provided the results from the experimental work that greatly assisted the present research.

References

[1] Lefebvre, A. H., Atomization and sprays (1988)
[2] Walzel, P., Chemie Ingenieur Technik 62: 983-994 (1990)
[3] Bayvel, L., Orzechowski, Z., Liquid Atomization (1993)
[4] Domnick, J., Thieme, M., Atomization and Sprays 16: 857-874 (2006)
[5] Domnick, J., Yang, Z., Ye, Q., 22nd European Conference on Liquid Atomization and Spray Systems, Lake Como, Italy, September 8-10 (2008)
[6] Shen, B., Ye, Q., Tiedje, O., Domnick, J., 28th European Conference on Liquid Atomization and Spray Systems, Valencia, Spain, September 6-8 (2017)
[7] Shen, B., Ye, Q., Tiedje, O., Domnick, J., 14th International Conference on Liquid Atomization and Spray Systems, Chicago, IL, USA, July 22-26 (2018)
[8] Mehrhardt, E., Ph.D. thesis, Technical University of Berlin (1978)
[9] Macosko, C. W., Rheology: Principles, Measurements, and Applications, Wiley-VCH (1994)